Current Theoretical Models and High Resolution Solar Observations: Preparing for ATST
ASP Conference Series, Vol. 286, 2003
A. A. Pevtsov and H. Uitenbroek, eds.

Physics of Photospheric Magnetic Field

A.A. van Ballegooijen

Harvard-Smithsonian Center for Astrophysics, 60 Garden Street, MS-15, Cambridge, MA 02138, USA

S.S. Hasan

Indian Institute of Astrophysics, Bangalore 560034, India

Abstract. The magnetic field on the quiet sun is continually swept into the intergranular lanes where it is amplified by interactions with the surrounding cool downflows. The resulting kilogauss flux tubes have typical sizes of about 100 km and magnetic field strengths of around 1500 G in the photosphere. A model of the magnetic field strength as function of depth is presented. It is shown that the Reynolds stress due to the downflows are sufficient to explain the observed kilogauss field strengths. We also present simulations of vorticity in intergranular lanes and the dynamics of flux tubes in response to such vortical motions. The simulations predict that flux tubes rotate with angular velocity $\sim 5\times10^{-3}$ rad/s. If true, this would likely result in a significant flux of Alfvén waves into the solar atmosphere that would contribute to the heating of the chromosphere and corona.

1. Introduction

The magnetic field on the quiet sun is highly intermittent, and contains kilogauss flux elements (Howard & Stenflo 1972; Frazier & Stenflo 1973). Sanchez Almeida & Lites (2000) argue that weak polarization signals account for most of the total (unsigned) magnetic flux, suggesting that a significant fraction of photospheric flux remains undetected. The magnetic field emerges in the form of ephemeral regions (Harvey & Martin 1973; Harvey 1993) and intranetwork fields (Livingston & Harvey 1975; Zirin 1987; Wang et al. 1995; Zhang et al. 1998). The field strength of intranetwork fields is $\sim$ 500 G, less than that of the kilogauss flux elements (Keller et al. 1994; Lin 1995; Lites 2002). Lin & Rimmele (1999) identify a pattern of weak fields that is closely associated with the solar granulation. Hanle measurements indicate the presence of weak "turbulent" fields that are ubiquitous and have field strengths in the range 4-40 G (Stenflo, Keller, & Gandorfer 1998). This wide range of field strengths is the result of interactions of the magnetic field with mass flows in the convection zone. Convective flows occur on a range of spatial scales, ranging from 30,000 km for supergranules down to 100 km or less for downflows in intergranular lanes. Subsurface magnetic fields are continually stretched and distorted by these con-

vective flows (e.g., Cattaneo 1999; Emonet & Cattaneo 2001). The resulting flux bundles rise up to the solar surface and emerge in the photosphere.

The quiet solar corona consists of a complex network of magnetic loops known as the "magnetic carpet" (Title & Schrijver 1998; Handy & Schrijver 2001). The newly emerged fields are swept towards the boundaries of granules and supergranules, where they interact with pre-existing magnetic fields. These interactions depend strongly on the polarity of the fields involved: like-polarity magnetic elements will merge into larger elements, whereas opposite-polarity elements may fully or partially "cancel" each other, leading to removal of magnetic flux from the photosphere (Livi, Wang, & Martin 1985). The continual emergence and disappearance of magnetic fields causes recycling of the photospheric magnetic flux. In mixed-polarity regions with mean flux density of a few Gauss the recycling time scale is about 40 hours (Title & Schrijver 1998). The physical processes associated with flux cancellation are not well understood. Harvey et al. (1999) suggest that magnetic flux is retracting below the surface at most, if not all, cancellation sites. Others have argued that flux cancellation involves the rise of U-loops through the photosphere (e.g., Spruit, Title, & van Ballegooijen 1987). In most cases the magnetic flux elements involved in the cancellation were not previously connected to each other, so magnetic reconnection is required above or below the surface to established the required loop-like connections between the cancelling features.

The magnetic field is continually swept into the intergranular lanes where it is amplified by interactions with the surrounding cool downflows. The resulting kilogauss "flux tubes" have typical sizes of about 100 km and magnetic field strengths of around 1500 G at the base of the photosphere. Figure 1 illustrates the structure of a flux tube and the surrounding flows. The flux tubes are less dense than their surroundings, so they are buoyant. This buoyancy keeps the flux tubes nearly vertically oriented in the photosphere despite the perturbing flows. The flux tubes can be modeled either as monolithic magnetic structures (e.g., Spruit 1976; Frutiger & Solanki 2001), or as micro-structured magnetic atmospheres (MISMAs) that contain fine structure on scales far below the resolution of present telescopes (Sanchez Almeida et al. 1996). The physical processes that determine the observed field strengths in flux tubes are discussed in section 2. We argue that the observed field strengths are determined by dynamical forces in the downflows near the solar surface.

The flux tubes follow the intergranular lanes as the convective pattern evolves. They continually split up and merge due to interactions with flows inside the lanes and with each other (e.g., Berger & Title 1996). It is unclear whether this splitting and merging leads to significant changes in field strength within the flux tubes. The motions of flux tubes within the intergranular lanes are likely to generate transverse MHD waves that propagate upward along the flux tubes and dissipate their energy in the chromosphere and corona (e.g., Huang, Musielak, & Ulmschneider 1995; Hasan & Kalkofen 1999; Hasan, Kalkofen, & van Ballegooijen 2000; Musielak & Ulmschneider 2002). At present there are no observational constraints on the properties of transverse waves (such as wave power spectra). Obtaining such knowledge is important for understanding the non-thermal heating of the upper solar atmosphere, and is one of the main goals of the Advanced Technology Solar Telescope (ATST).

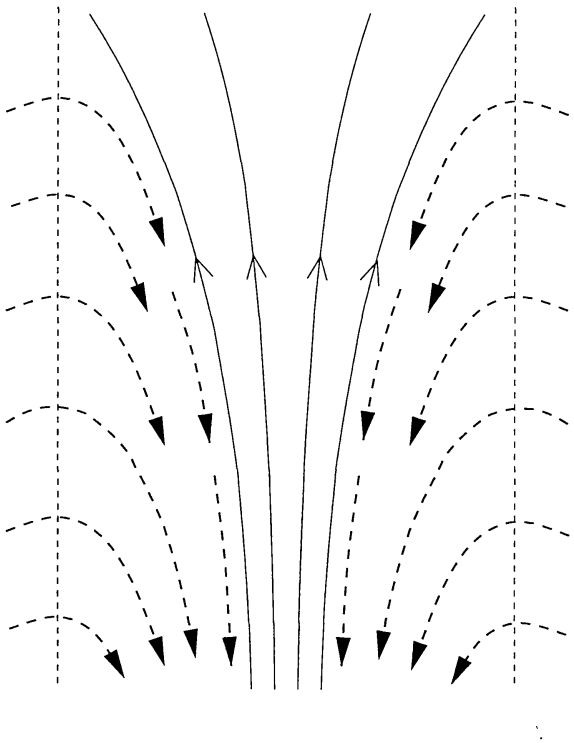

Figure 1. Magnetic flux tube with downflows in local surroundings.

In section 3 we present a simple model of the interaction between flux tubes and the flows associated with the solar granulation. We find that the *vorticity* of the flow plays an important role in the dynamics of the flux tubes. Like the magnetic flux, the vertical vorticity is concentrated in the intergranular lanes and therefore interacts strongly with the magnetic flux tubes (Schüssler 1984, 1986). The model predicts rotational motions of flux tubes with angular velocity of around 5×10^{-3} rad/s. Such motions would have important effects on the dynamics of magnetic field in the upper solar atmosphere.

2. Magnetic Field Strength of Flux Tubes

A large fraction of the magnetic flux on the quiet sun consists of highly concentrated kilogauss fields (e.g., Howard & Stenflo 1972; Frazier & Stenflo 1973). The formation of kilogauss flux tubes by convective collapse (CC) of an initially weak magnetic field has been investigated by many authors (see Rajaguru & Hasan 2000, and references therein). The CC is due to the unstable stratification of the convection zone. A flux tube with weak magnetic field in thermal and hydrostatic equilibrium with its surroundings is unstable against vertical displacements of plasma within the tube. If the displacements are downward, the flux tube is evacuated and may reach a new equilibrium state with higher field strength (Parker 1978; Spruit 1979; Spruit & Zweibel 1979). Rajaguru & Hasan (2000) found that the CC of a flux tube is strongly influenced by radiative heating from the surroundings and cooling due to losses in the vertical direction.

Flux concentrations with magnetic fluxes in excess of 10^{18} Mx collapse unhindered, attaining field strengths greater than 1160 G, but for smaller magnetic fluxes the CC is inhibited by radiation transport effects.

In the CC model the horizontal variations of temperature in the external medium are ignored, and the medium is assumed to be in hydrostatic equilibrium. However, we know that the flux tubes are located in cool intergranular lanes where the temperature $T_d(z)$ is less than the average temperature $T_e(z)$ at depth z in the convection zone. Moreover, there are strong downflows that cause deviations from hydrostatic equilibrium. These deviations can be described in two complementary ways. Sanchez Almeida (2001) focuses on the temperature deficit of the downflows. He assumes that the downflows are in pressure balance with the mean atmosphere, $p_d(z) \approx p_e(z)$, and that the mean atmosphere is approximately in hydrostatic equilibrium, $dp_e/dz \approx p_e/H_e$, where $H_e(z) \equiv RT_e/\mu_e g$ is the pressure scale height, $\mu_e(z)$ is the molecular weight, and g is the acceleration of gravity. Since $T_d < T_e$, the pressure gradient in the downflow is less steep than necessary to compensate gravity, i.e., there are negative buoyancy forces that drive the downdrafts in intergranular lanes. To determine the temperature of the downflows, Sanchez Almeida (2001) used simulation results from a realistic three-dimensional model of solar convection by Stein & Nordlund (1998). Another approach is to consider the momentum equation for the downflow (Hasan & van Ballegooijen 1998):

$$\frac{d}{dz}\left(p_d + \rho_d v_d^2\right) = \rho_d g = \frac{p_d}{H_d}, \tag{1}$$

where $v_d(z)$ is the average downward velocity, $p_d(z)$ and $\rho_d(z)$ are the average pressure and density of the downflow, and $H_d(z)$ is the pressure scale height that would exist if the medium were in hydrostatic equilibrium ($H_d \equiv RT_d/\mu_d g$). The advantage of this approach is that it makes no assumptions about the mean stratification of the convection zone. Equation (1) is an approximation that can be derived by averaging the vertical component of the momentum equation over the downflow region (indicated by dashed lines in Fig. 1). The cross-sectional area of the downflows is assumed to be independent of depth.

The deviations from hydrostatic equilibrium in the downflows have important consequences for magnetic flux tubes that are embedded in such flows (Hasan & van Ballegooijen 1998; Sanchez Almeida 2001). The gas inside the flux tube is assumed to be in hydrostatic equilibrium along the field lines:

$$\frac{dp_i}{dz} = \rho_i g = \frac{p_i}{H_i}, \tag{2}$$

where $p_i(z)$ and $\rho_i(z)$ are the internal gas pressure and density, and $H_i \equiv RT_i/\mu_i g$. Furthermore, we use the thin tube approximation (Roberts & Webb 1978; Spruit 1981), which implies that the flux tube is in pressure balance with its surroundings:

$$p_i + \frac{B^2}{8\pi} = p_d, \tag{3}$$

where $B(z)$ is the magnetic field strength. This approximation is valid when the radius of the flux tubes is less than the pressure scale height ($H_d \approx 100$ km in

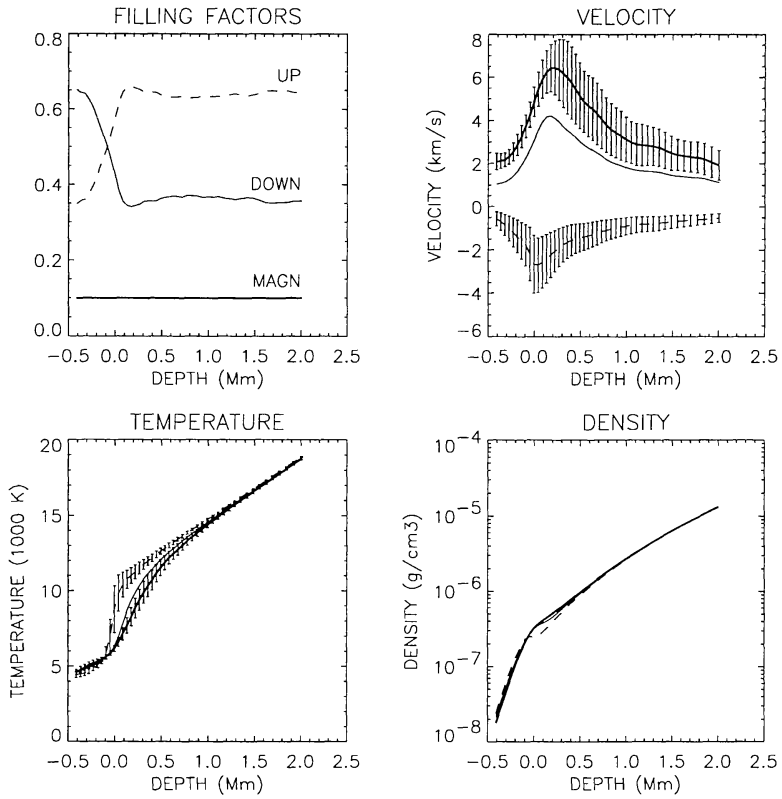

Figure 2. Filling factors, velocities, temperatures and densities for upflows (*dashed* curves), downflows (*thin solid* curves), and the fraction of area with the strongest downflows (*thick solid* curves), as derived from the convection simulation by Stein & Nordlund (1998).

the photosphere). Combining the above equations yields

$$\frac{d}{dz}\ln(1+\epsilon) = \left(\frac{1}{H_d} - \frac{1}{H_i}\right) - \frac{1}{p_d}\frac{d}{dz}\left(\rho_d v_d^2\right), \tag{4}$$

where $\epsilon \equiv B^2/(8\pi p_i)$ is the ratio of magnetic pressure to gas pressure (the inverse of the plasma parameter β). It follows that the magnetic pressure inside flux tubes is determined by two effects: (1) the temperature deficit or excess of the flux tube relative to its surroundings; and (2) the Reynolds stresses in the surroundings. The temperature effect is described by the first term in equation (4). A temperature deficit ($T_i < T_d$) can occur due to radiative cooling at the solar surface, but this effect is expected to be important only for relatively thick flux tubes (with radii r larger than the pressure scale height, which is about 100 km at $z = 0$), and then only for depths $z < r$ (Spruit 1976). Then $H_i < H_d$, so the first term in equation (4) is negative. However, very thin flux tubes are expected to be in thermal equilibrium with their surroundings ($H_i \approx H_d$), so that the first term in equation (4) vanishes.

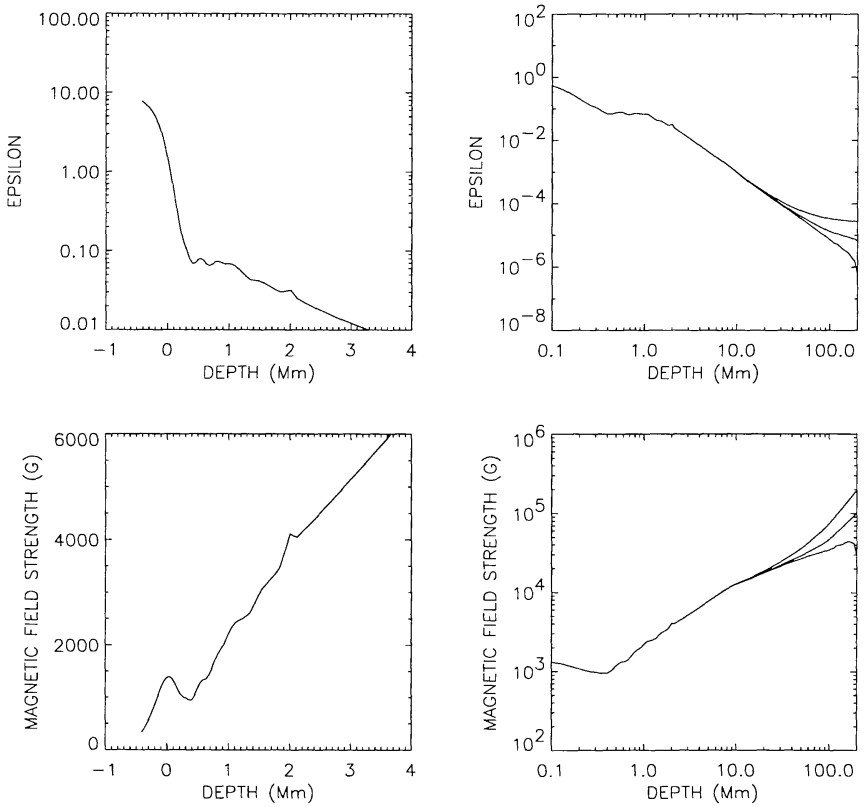

Figure 3. The ratio of magnetic- and gas pressure, $\epsilon(z)$, and magnetic field strength, $B(z)$, as functions of depth in the convection zone.

The Reynolds-stress effect is described by the second term in equation (4). Since $\rho_d v_d^2$ increases with depth, its effect is to make $\epsilon(z)$ a decreasing function of depth. To determine the magnitude of the Reynolds stress, we derive average properties of the downflows from the convection model by Stein & Nordlund (1998). Using a snapshot from their simulation model, we determine the average velocity, temperature and density as functions of depth for (1) upflows, (2) downflows, and (3) the 10% fraction of the total area with the strongest downflows. The latter is a measure of the local surroundings of the flux tubes, which presumably are located in the core of the downflow plumes. The results of this analysis are shown in Fig. 2, together with the area-filling factor as a function of depth for each region. Note that the strongest downflows occur at a depth of about 200 km and have a velocity of about 6 km/s. To extend these results to greater depth ($z > 2000$ km), we use a model for the mean stratification of the convection zone (Spruit 1977) and a two-component model of convective energy transport based on downward directed plumes embedded in a gentle upflow (Hasan & van Ballegooijen 1998). The parameters of this plume model are adjusted to match the numerical results from Stein & Nordlund (1998) at a depth $z \approx 2000$ km.

To determine the magnetic field strength as a function of depth, equation (4) is solved numerically by integrating upward from the base of the convection zone, assuming $H_i(z) = H_d(z)$. Three different values for the field strength at the base are used, $B_0 = 30$, 100, and 200 kG. The results for the pressure ratio $\epsilon(z)$ and magnetic field strength $B(z)$ are shown in Fig. 3. Note that $\epsilon(z)$ increases with decreasing depth from $\epsilon \sim 10^{-5}$ at large depth in the convection zone to $\epsilon \approx 5$ in the photosphere. Most of the increase in ϵ occurs close to the solar surface ($-300 < z < +300$ km) where the Reynolds stresses are relatively large. The value of $\epsilon(z)$ in the upper part of the convection zone is nearly independent of the assumed field strength at the base. The predicted field strength at $z = 0$ is about 1380 G, consistent with the observed values in flux tubes on the quiet sun (e.g., Zayer et al. 1990; Grossmann-Doerth, Keller, & Schüssler 1996). This implies that Reynolds stresses due to downflows are sufficient for reproducing the observed field strengths, and there is no need to invoke temperature deficits of the flux tubes relative to their local surroundings.

Note that the predicted field strength (1380 G) is significantly larger than the "equipartition" value $B_{eq} \sim 400$ G in the photosphere (equipartition between magnetic and kinetic energy densities). This is due to the cumulative effect of the downflows over several pressure scale heights. Therefore, incompressible magneto-convection simulations (e.g., Emonet & Cattaneo 2001) do not necessarily give an accurate view of the formation of kilogauss flux elements.

3. Simulation of Granulation Flow and Flux Tube Motion

The motions of photospheric flux tubes are mainly determined by the evolving granulation flow. The buoyancy of a flux tube guarantees that it remains nearly vertical, hence its position on the solar surface is determined by the average horizontal velocity acting upon the flux tube in the upper part of the convection zone. To follow a large number of flux tubes we need to know the velocity field, $\mathbf{v} \equiv [v_x(x, y, t), v_y(x, y, t)]$, where x and y are coordinates on the solar surface, and t is the time. In principle this velocity field can be estimated from a time-series of granulation images. However, the spatial resolution of present telescopes is insufficient to track small features within granules and intergranular lanes. To derive a flow field from granulation images additional information about the velocity is required. In previous work we assumed for simplicity that the vorticity of the flow vanishes, so that the velocity can be approximated by $\mathbf{v} = -\nabla\phi$, where $\phi(x, y, t)$ is the flow potential (van Ballegooijen et al. 1998, hereafter paper I). The quantity ϕ is assumed to be well correlated with the granulation intensity (positive in the bright granules and negative in the intergranular lanes), so that $-\nabla\phi$ represents the radial outflow from the cell center to the lanes. However, in reality the vorticity of the flow may not be negligible.

To study the role of vorticity in the dynamics of flux tubes, we add a random vorticity source to the model described in paper I. The flow velocity $\mathbf{v}$ is computed from the following equation:

$$\frac{\partial \mathbf{v}}{\partial t} + \mathbf{v} \cdot \nabla \mathbf{v} = -\nabla p + \hat{\mathbf{z}} \times \nabla q + \nu \nabla^2 \mathbf{v} - \frac{\mathbf{v}}{\tau}, \tag{5}$$

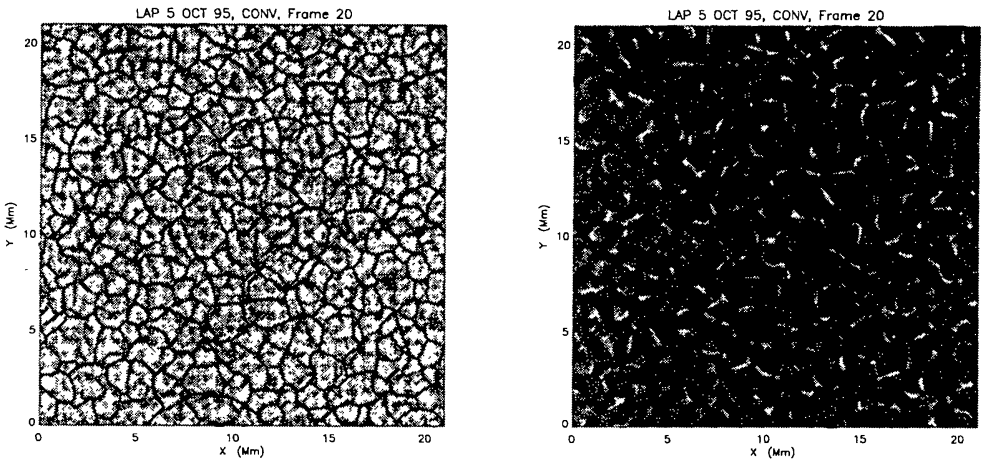

Figure 4. Divergence and vorticity of horizontal flows.

where $p(x, y, t)$ is proportional to observed granulation intensity:

$$p(x, y, t) = c_1 I_{\rm obs}(x, y, t), \tag{6}$$

and $q(x, y, t)$ is a random vorticity source (we use $\nu = 70$ km^2/s and $\tau = 500$ s). The granulation images were obtained at the Swedish Vacuum Solar Telescope, La Palma, on 1995 October 5 (see Löfdahl et al. 1998; Berger et al. 1998). The random vorticity source $q(x, y, t)$ has a correlation length of 600 km and correlation time of 71 s. We experimented with different values of the strength of the vorticity source as measured by the rms value of the parameter q. In each case the constant c_1 was determined by comparing the rms values of v_x and v_y with those predicted by the 3D hydro-dynamical simulations of Stein & Nordlund (1998), similar to the procedure described in paper I. Here we present results only for one value of the vorticity source, $q_{rms} = p_{rms} = 3.2$ km^2/s^2. Figure 4 shows the spatial distribution of divergence and vorticity for frame 50 of the time series. Note that the vorticity is strongly concentrated in the intergranular lanes (dark lines in divergence image), despite the fact that the vorticity source was much more evenly distributed. This is due to the "bathtub effect": vorticity fluctuations are advected into narrow downflow regions, leading to spin up of the flow (Schüssler 1986). The presence of vortical flows around flux tubes may help to stabilize the flux tubes against interchange instability (Schüssler 1984).

We now consider the dynamics of flux tubes in this evolving flow pattern. The flux tubes are represented by 200 finite-size corks (radius 60 km) that move with the granulation flow. The corks are not allowed to overlap; this simulates the incompressibility of kilogauss fields in the photosphere (for details, see paper I). Initially, the corks are randomly distributed in a square with a size of 5000 km. Figure 5 shows their positions at later times. Unlike in paper I, the corks have rotational motions given by the local vorticity of the granulation flow, $\Omega_k(t) = (\nabla \times \mathbf{v})_z/2$. We find that the rotation rates are quite large, $\Omega_{rms} \sim 5 \times 10^{-3}$ rad/s, i.e., a rotation over 1 radian in only 200 s.

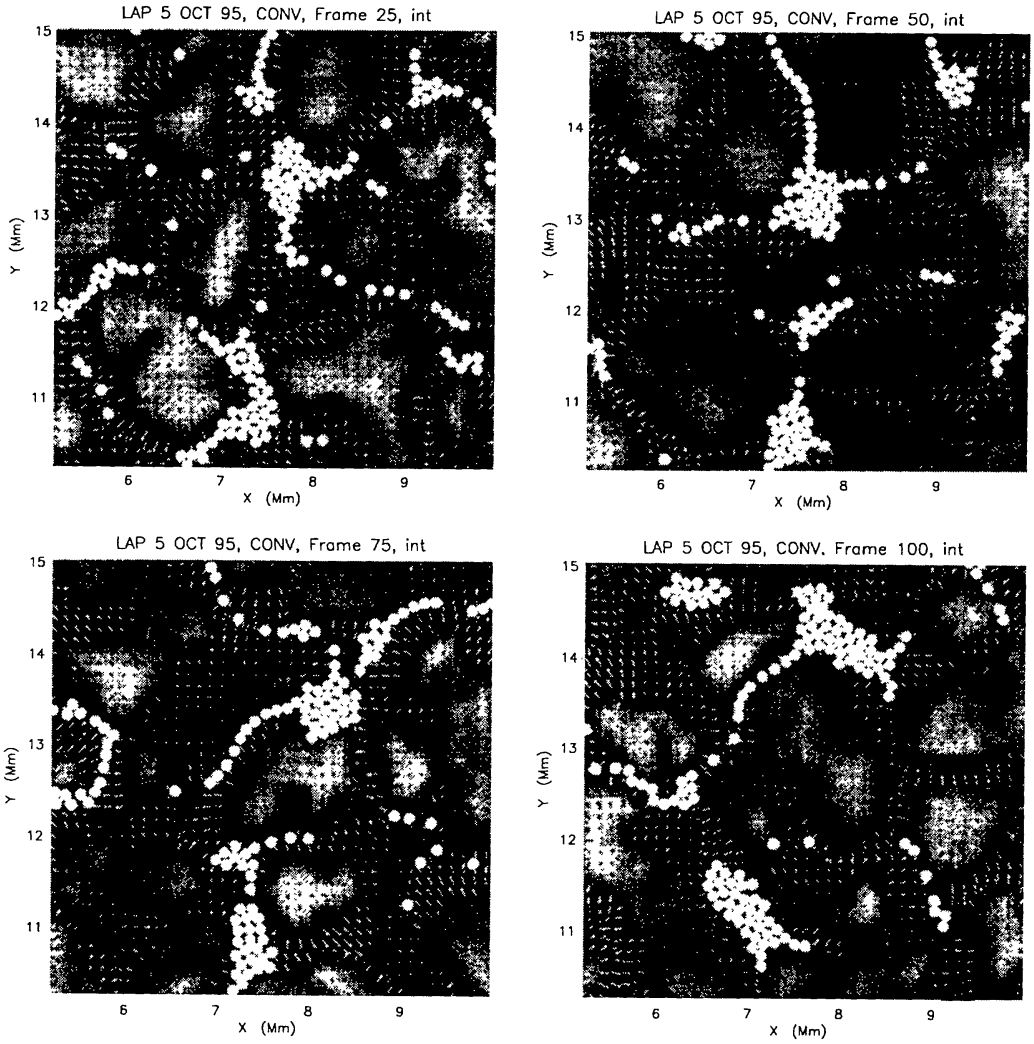

Figure 5. Cork positions at times $t = 9.4$, 19.2, 30.0 and 38.8 min.

If such rotational motions of flux tubes indeed occur on the Sun, this could have important consequences for the dynamics of magnetic fields and plasma in the upper solar atmosphere. The magnetic field is frozen into the plasma, hence any rotational motions imposed from below will propagate up along the flux tubes in the form of Alfvén waves. Since the flux tubes fan out with height, the rotational velocity is enhanced by the expansion factor. To estimate the magnitude of this effect, we now simulate the motions of magnetic field lines attached to the corks using potential-field extrapolation. Each cork is replaced by a magnetic source located at depth $z = 160$ km below the photosphere (all sources have the same strength and polarity). Each source consists of a magnetic monopole and a vertically oriented bipole; this produces a magnetic "canopy" located at a height of 1000 km above the level $z = 0$ (see paper I). The total

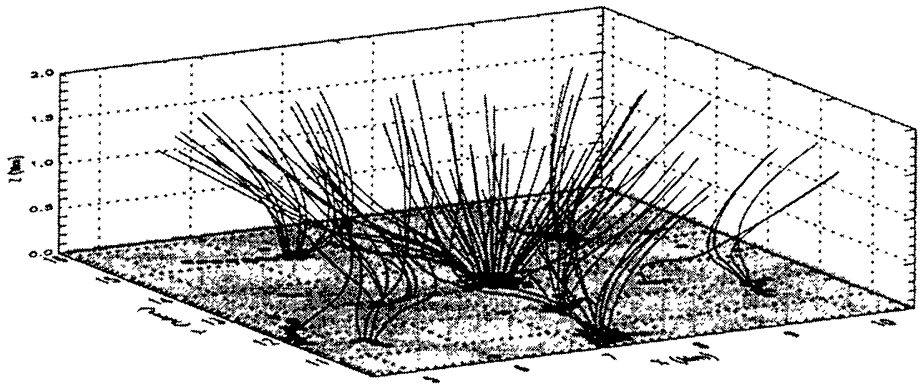

Figure 6. Potential field derived from cork simulation ($t = 19.2$ min).

magnetic field $\mathbf{B}$ is computed as the sum over all magnetic sources:

$$\mathbf{B}(\mathbf{r},t) = \sum_k \mathbf{B}_k(\mathbf{r},t). \tag{7}$$

Flux tubes are defined by tracing field lines downward from a height of 1500 km in the chromosphere. The flux tubes are pushed up against each other in the chromosphere, but there are "field-free" regions below the canopy. Figure 6 shows selected field lines at time $t = 19.2$ min.

The chromospheric field-line velocity is computed by using the frozen-in condition, $\mathbf{E} + \mathbf{v} \times \mathbf{B} = 0$, in combination with Faraday's law:

$$\nabla \times \mathbf{E} = -\frac{\partial \mathbf{B}}{\partial t} = -\sum_k \frac{\partial \mathbf{B}_k}{\partial t} = \sum_k \nabla \times \mathbf{E}_k, \tag{8}$$

where $\mathbf{E}_k(\mathbf{r},t)$ is the electric field from a single source:

$$\mathbf{E}_k(\mathbf{r},t) \equiv -\left[\mathbf{v}_k(t) + \Omega_k(t)\ \hat{\mathbf{z}} \times (\mathbf{r} - \mathbf{r}_k(t))\right] \times \mathbf{B}_k(\mathbf{r},t). \tag{9}$$

Here $\mathbf{r}_k(t)$ is the source position, $\mathbf{v}_k(t) \equiv d\mathbf{r}_k/dt$ is its velocity, and $\Omega_k(t)$ is the rotation rate. Then the electric field can be written as

$$\mathbf{E}(\mathbf{r},t) = \sum_k \mathbf{E}_k(\mathbf{r},t) - \nabla\Phi, \tag{10}$$

where $\Phi(\mathbf{r},t)$ is determined by the requirement that $\mathbf{E} \cdot \mathbf{B} = 0$:

$$\mathbf{B} \cdot \nabla\Phi = \sum_k \mathbf{B} \cdot \mathbf{E}_k. \tag{11}$$

Equation (11) is solved by integrating downward along the field lines and setting $\Phi(x,y,0,t) = 0$ in the photosphere. This yields the function $\Phi(\mathbf{r},t)$ in the

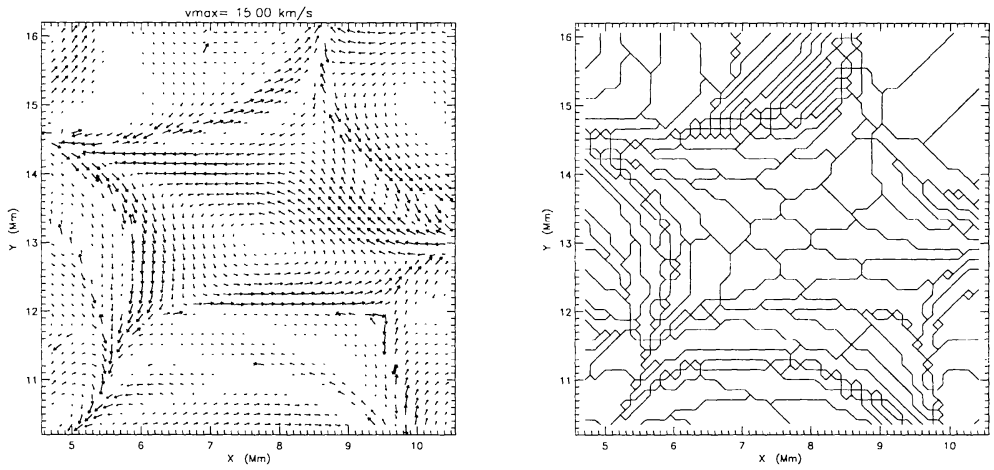

Figure 7. Field-line velocity at height 1500 km in the chromosphere as predicted by potential-field extrapolation and the assumption that the magnetic field is frozen into the plasma. (a) Horizontal component of velocity for $t = 19.2$ min. The thick arrows correspond to velocities in excess of 15 km/s. (b) Magnetic domains associated with each cork.

chromosphere, from which the electric field $\mathbf{E}(\mathbf{r}, t)$ and the field-line velocity $\mathbf{v}(\mathbf{r}, t) = \mathbf{E} \times \mathbf{B}/B^2$ can be computed. Figure 7a shows the field-line velocity for time $t = 19.2$ min of the simulation (Fig. 6). Note the rotational pattern associated with the flux element in the center of Fig. 6. Figure 7b shows the magnetic domains associated with each cork. Note that these domains are elongated for corks near the boundaries between flux bundles where the largest velocities occur. It was previously suggested that local enhancements of field-line velocity near separatrix surfaces between neighboring flux tubes are the cause of spicules (van Ballegooijen & Nisenson 1999).

Figure 8 shows histograms of the horizontal and vertical velocity components. The velocity distributions are fit by exponential distributions with $1/e$ widths of 5.4 and 3.7 km/s, respectively. Such velocities are consistent with observed non-thermal line broadening of spectral lines formed in the chromosphere and transition region (Dere & Mason 1993). However, it should be kept in mind that the rate of vorticity input in our model is rather arbitrary and is not constrained by actual observations of vorticity.

4. Conclusions

The observed kilogauss fields in the photosphere are due to deviations from hydrostatic equilibrium in the local surroundings of flux tubes (Hasan & van Ballegooijen 1998; Sanchez Almeida 2001). These deviations are due to the strong downdrafts ($v_z \sim 6$ km/s) as predicted by hydro-dynamic convection models (Stein & Nordlund 1998). Here we use simulation results from Stein & Nordlund's model to estimate the Reynolds stress in the downflow, and we find that the observed field strength can be reproduced without invoking temperature

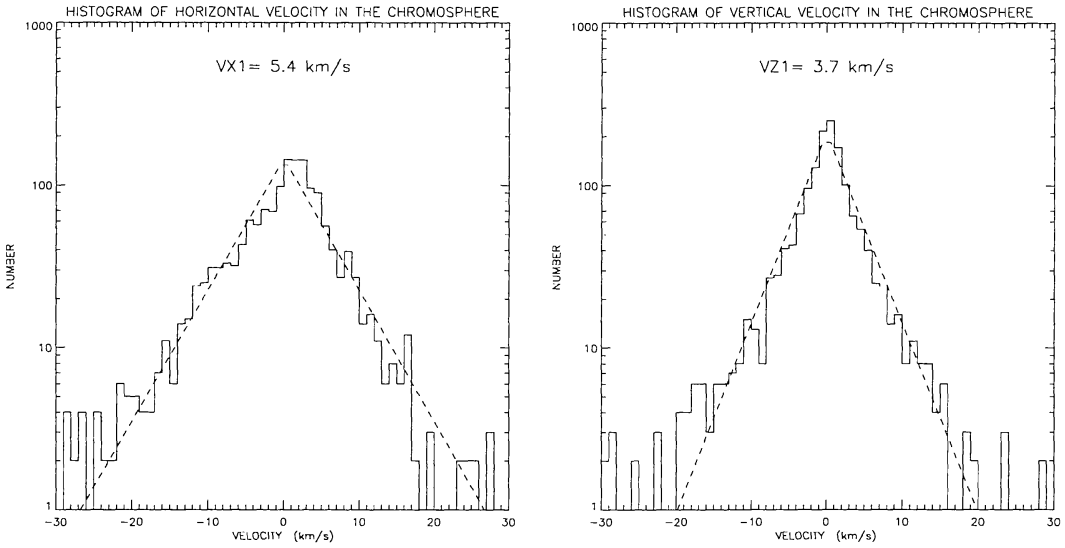

Figure 8. Histograms of horizontal and vertical velocity in the chromosphere (frame 50, height $z = 1500$ km).

deficits of the flux tubes relative to their local surroundings. The predicted field strength (1380 G at $z = 0$ in the photosphere) is much larger than the "equipartition" value; this is due to the cumulative effect of the downflows over several pressure scale heights. The downflows are also needed to account for the observed Stokes-V profile asymmetries (e.g., Frutiger & Solanki 2001).

Little is known about the vorticity of granulation flows on length scales comparable to the width of an intergranular lane ($\sim$ 200 km). Here we simulate the effects of vorticity on the dynamics of flux tubes by adding a random vorticity source to the granulation model developed in paper I. This model is based on a time-series of granulation images obtained with the SVST at La Palma. We find that the flux tubes may have significant rotation rates, $\Omega \sim 5 \times 10^{-3}$ rad/s. It is unclear whether such rapid rotational motions indeed occur on the Sun; a more systematic search for vorticity in intergranular lanes is needed to settle this issue. We also extrapolate the predicted velocities to larger heights in the solar atmosphere, and predict field-line motions in the chromosphere with mean velocities of several km/s.

Acknowledgments. We thank R. Stein and Å. Nordlund for providing results from their hydro-dynamical simulations of solar convection.

References

Berger, T. E., Löfdahl, M. G., Shine, R. A., & Title, A. M. 1998, ApJ, 495, 973

Berger, T. E., & Title, A. M. 1996, ApJ, 463, 365

Cattaneo, F. 1999, ApJ, 515, L39

Dere, K. P., & Mason, H. E. 1993, Solar Phys., 144, 217

Emonet, T., & Cattaneo, F. 2001, ApJ, 560, L197

Frazier, E. N., & Stenflo, J. O. 1972, Solar Phys., 27, 330

Frutiger, C., & Solanki, S. K. 2001, A&A, 369, 646

Grossmann-Doerth, U., Keller, C. U., & Schüssler, M. 1996, A&A, 315, 610

Handy, B. N., & Schrijver, C. J. 2001, ApJ, 547, 1100

Harvey, K. L. 1993, Magnetic Bipoles on the Sun, Ph.D. Thesis (Utrecht), Chapters 5 and 6

Harvey, K. L., Jones, H. P., Schrijver, C. J., & Penn, M. J. 1999, Solar Phys., 190, 35

Harvey, K. L., & Martin, S. F. 1973, Solar Phys., 32, 389

Hasan, S. S., & Kalkofen, W. 1999, ApJ, 519, 899

Hasan, S. S., Kalkofen, W., & van Ballegooijen, A. A. 2000, ApJ, 535, L67

Hasan, S. S., & van Ballegooijen, A. A. 1998, in ASP Conf. Ser. Vol. 154, The Tenth Cambridge Workshop on Cool Stars, Stellar Systems and the Sun, ed. R. A. Donahue & J. A. Bookbinder (San Francisco: ASP), 630

Howard, R. W., & Stenflo, J. O. 1972, Solar Phys., 22, 402

Huang, P., Musielak, Z. E., & Ulmschneider, P. 1995, A&A, 297, 579

Keller, C. U., Deubner, F.-L., Egger, U., Fleck, B., & Povel, H. P. 1994, A&A, 286, 626

Lin, H. 1995, ApJ, 446, 421

Lin, H., & Rimmele, T. 1999, ApJ, 514, 448

Lites, B. W. 2002, ApJ, 573, 431

Livi, S. H. B., Wang, J., & Martin, S. F. 1985, Aust. J. Phys., 38, 855

Livingston, W. C., & Harvey, J. W. 1975, BAAS, 7, 346

Löfdahl, M. G., Berger, T. E., Shine, R. A., & Title, A. M. 1998, ApJ, 495, 965

Musielak, Z. E., & Ulmschneider, P. 2002, A&A, 386, 606

Parker, E. N. 1978, ApJ, 221, 368

Rajaguru, S. P., & Hasan, S. S. 2000, ApJ, 544, 522

Roberts, B., & Webb, A. R. 1978, Solar Phys., 56, 5

Sanchez Almeida, J. 2001, ApJ, 556, 928

Sanchez Almeida, J., Landi degl'Innocenti, E., Martinez Pillet, V., & Lites, B. W. 1996, ApJ, 466, 537

Sanchez Almeida, J., & Lites, B. W. 2000, ApJ, 532, 1215

Schüssler, M. 1984, A&A, 140, 453

Schüssler, M. 1986, in Small Scale Magnetic Flux Concentrations in the Solar Photosphere, ed. W. Deinzer, M. Knölker, & H. H. Voigt (Göttingen: Vandenhoeck & Rupert), 103

Spruit, H. C. 1976, Solar Phys., 50, 269

Spruit, H. C. 1977, Magnetic Flux Tubes and Transport of Heat in the Convection Zone of the Sun, Ph.D. Thesis (Utrecht), Chapter 2

Spruit, H. C. 1979, Solar Phys., 61, 363

Spruit, H. C. 1981, A&A, 102, 129

Spruit, H. C., Title, A. M., & van Ballegooijen, A. A. 1987, Solar Phys., 110, 115

Spruit, H. C., & Zweibel, E. G. 1979, Solar Phys., 62, 15

Stein, R. F., & Nordlund, Å. 1998, ApJ, 499, 914

Stenflo, J. O., Keller, C. U., & Gandorfer, A. 1998, A&A, 329, 319

Title, A. M., & Schrijver, C. J. 1998, in ASP Conf. Ser. Vol. 154, The Tenth Cambridge Workshop on Cool Stars, Stellar Systems and the Sun, ed. R. A. Donahue & J. A. Bookbinder (San Francisco: ASP), 345

van Ballegooijen, A. A., Nisenson, P., Noyes, R. W., Löfdahl, M. G., Stein, R. F., Nordlund, Å., and Krishnakumar, V. 1998, ApJ, 509, 435 (paper I)

van Ballegooijen, A. A., & Nisenson, P. 1999, in ASP Conf. Ser. Vol. 183, High Resolution Solar Physics: Theory, Observations, and Techniques, ed. T. R. Rimmele, K. S. Balasubramaniam & R. R. Radick (San Francisco: ASP), 30

Wang, J., Wang, H., Tang, F., Lee, J. W., & Zirin, H. 1995, Solar Phys., 160, 277

Zhang, J., Lin, G., Wang, J., Wang, H., & Zirin, H. 1998, A&A, 338, 322

Zayer, I., Solanki, S. K., Stenflo, J. O., & Keller, C. U. 1990, A&A, 239, 356

Zirin, H. 1987, Solar Phys., 110, 101